WELDING RESEARC H

SUPPLEMENT TO THE WELDING JOURNAL, DECEMBER 2001
Sponsored by the American Welding Society and the Welding Research Council

Interstitial Diffusion of Carbon and Nitrogen into Heat-Affected Zones of 11–12% Chromium Steel Welds

The possibility of introducing austenite stabilizers into the HAZ to restrict grain growth is investigated

BY A. M. MEYER AND M. du TOIT

ABSTRACT. The welding of 11–12% chromium steels is subject to the traditional concern with ferritic grain growth in the heat-affected zone of ferritic stainless steels. The grain growth could be inhibited if austenite on the ferrite grain boundaries could be stabilized at high temperatures.

This article discusses the possibility that diffusion from the weld metal can increase the carbon or nitrogen content of the heat-affected zone, and consequently stabilize grain boundary austenite.

Introduction

In recent years, considerable interest has developed in the use of 3CR12 by the automotive and agricultural industries (Ref. 1). The cost of additional thickness requirements and surface treatments needed to counteract corrosion loss in conventional carbon steel presents a large portion of the material cost over the life cycle of a component. The interest in 3CR12, therefore, arises from its relative resistance to atmospheric corrosion (Ref. 1). The chemical composition of this corrosion-resistant steel is shown in Table 1. However, the traditional concerns regarding grain growth and embrittlement in the heat-affected zones of welds in ferritic stainless steels also apply to 3CR12.

The heat-affected zone in 3CR12 consists of three zones, namely the high-temperature heat-affected zone (HTHAZ), the duplex zone and the low-temperature heat-affected zone (LTHAZ) (Ref. 2). The grain growth that occurs in the HTHAZ during welding is the main cause of concern. The phase composition of the heat-affected zone at high temperatures depends on the relative amount of austenite and ferrite stabilizers in the steel (Ref. 3). During cooling, grain growth is restricted by grain boundary austenite (Ref. 3). Considerable ferrite grain growth occurs during the heating cycle and close to the peak temperature when the phase composition is fully ferritic (Ref. 3).

The research done for this article explores the possibility of introducing austenite stabilizers into the heat-affected zone during welding to restrict grain growth through forming a dual-phase ferritic-austenitic structure close to the peak temperature reached during welding. The width of the heat-affected zone is a function of the heat input during welding (Ref. 4).

KEY WORDS

Austenite
Ferrite
HAZ
Ferritic Stainless
Grain Growth
Embrittlement

The Influence of Ferrite Grain Size on Impact Properties

Ferrite grain size has a marked effect on the impact properties of the HTHAZ. Ductile-to-brittle-transition-temperature (DBTT) results from samples obtained through temperature-cycle simulation by Gooch and Ginn (Ref. 5) indicate the DBTT of 12% ferritic-martensitic steel increases with the ferrite grain size.

The Petch relationship between transition temperature and grain size is given by the form (Ref. 5)

$$DBTT = F + G\ln(d^{-1/2}) \quad (1)$$

where F and G are constants and d is the grain diameter.

The DBTT results obtained by Gooch and Ginn (Ref. 5) are plotted against $\ln(d^{-1/2})$ in Fig. 1. An approximate correlation with Equation 1 was found. This indicates the ferrite grain size would play a major role in the fracture toughness of the HTHAZ in 3CR12 welds.

The Influence of Martensite

It is well established that grain growth may only account for part of the observed

A. M. MEYER is with Metpro, a Division of Dorbyl, Pretoria, South Africa. M. du TOIT is with the Dept. of Materials Science and Metallurgical Engineering, University of Pretoria, South Africa.

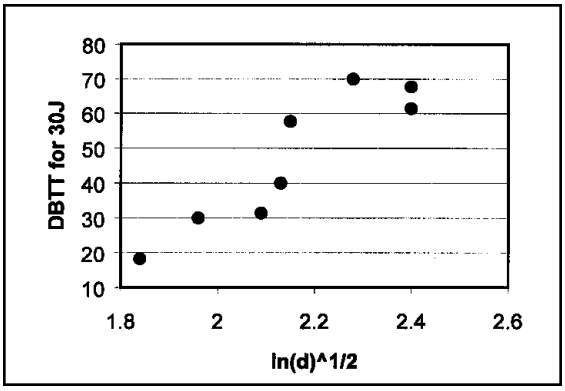

Fig. 1 — The effect of ferrite grain size on the toughness of 12% ferritic-martensitic steels (Ref. 5).

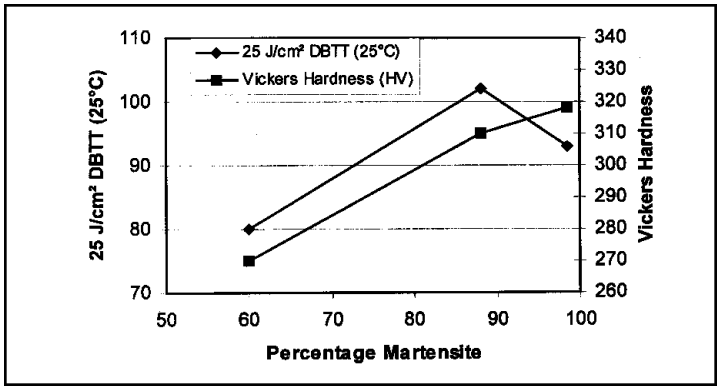

Fig. 2 — The influence of martensite content on the DBTT of 11–12% chromium steel (Ref. 3).

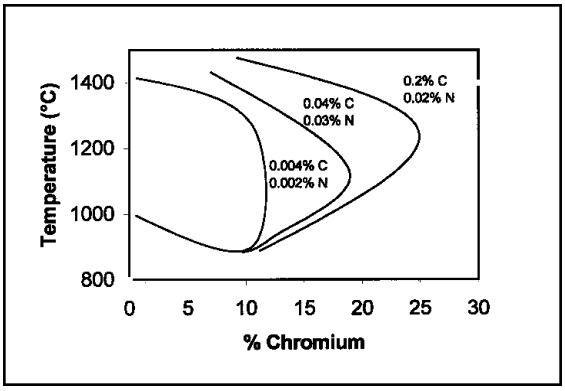

Fig. 3 — The influence of carbon and nitrogen on the size of the γ loop in the Fe-Cr system (Ref. 3).

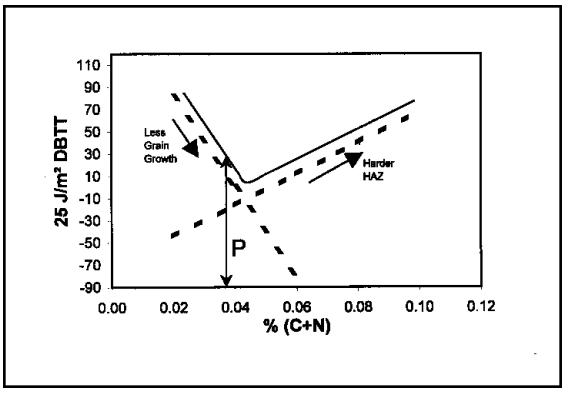

Fig. 4 — The effect of carbon and nitrogen content on the DBTT of the predominantly martensitic matrix (Ref. 3).

loss of toughness in the heat-affected zone of welded 3CR12 (Refs. 2, 3, and 5). Gooch and Ginn (Ref. 5) observed a general trend for transition temperatures to increase with higher martensite contents in microstructures dominated by high-temperature δ ferrite. They observed cleavage facets to have originated from martensite colonies. Intergranular martensite will inhibit the transmission of slip from one grain to the next, and act as an internal stress raiser (Ref. 5). It would thus seem likely the presence of martensite in a predominantly ferritic structure would facilitate cleavage fracture.

These comments assume fracture occurs in a predominantly ferritic structure. The mechanism could be quite different when martensite is the principal phase. Metallographic examination by Gooch and Ginn (Ref. 5) showed secondary cleavage to be arrested at martensite colonies. Due to this effect, the total energy absorbed during fracture will increase at higher martensite contents. The delta ferrite grain growth at high temperatures will also be restricted by a higher fraction of austenite on the grain boundaries (that would transform to martensite on cooling) (Ref. 5). Improved toughness should thus be obtained at higher fractions of martensite provided the structure is already predominantly martensitic.

The above-mentioned effect was observed in temperature simulation experiments executed by Zaayman (Ref. 3). Different amounts of martensite were obtained by applying different thermal cycles to samples of the same alloy. The results in Fig. 2 indicate an increasing fraction of martensite is harmful to the impact properties up to 90% martensite. The DBTT starts to decrease at 90% martensite, and continues to decrease as the fraction of martensite increases further. The martensite raises the stress in the softer ferrite at a martensite fraction of less than 90% (Ref. 3), and the higher stressed ferrite benefits cleavage fracture. Simultaneously, however, an increase in the fraction of martensite decreases the grain size of the remaining ferrite. This refining effect dominates at martensite fractions of more than 90% and this accounts for the observed decrease in DBTT (Ref. 3).

The Influence of Carbon and Nitrogen

Carbon and nitrogen affect the impact properties of the heat-affected zone in 11-12% chromium steels in two different ways. First, the hardness of the intergranular martensite that forms in the high temperature heat-affected zone increases with increasing carbon and nitrogen contents, which is harmful to the impact properties. Second, both carbon and nitrogen are strong austenite stabilizers and can restrict δ-ferrite grain growth by producing a dual phase at the high peak temperatures reached during welding (Ref. 3). The expansion of the austenite loop (γ loop) on the iron-chromium phase diagram can be seen in Fig. 3.

Table 1 — The Chemical Composition of 3CR12

Element	C	Cr	Si	Mn	Ni	N
Mass %	0.03 max	11–12	1.00 max	1.50 max	1.50 max	0.03 max

An optimum amount of carbon and nitrogen exists where the detrimental effect of a harder heat-affected zone exceeds the beneficial effect of a finer structure (Ref. 3). The ideal amount of carbon and nitrogen is strongly dependent on the content of other alloying elements, and therefore varies considerably (Ref. 3). The combined effect of carbon and nitrogen is shown in Fig. 4. The line P indicates the carbon and nitrogen levels of the base metal.

The Diffusion of Carbon and Nitrogen into the Heat-Affected Zone

A small addition of nitrogen to 3CR12 could restrict the δ-ferrite grain growth in the high-temperature heat-affected zone through the promotion of a dual phase at high temperatures. As discussed earlier, too much nitrogen would be detrimental to the impact properties. Therefore, it would be preferred if the nitrogen content could be increased locally in the vicinity of the weld. Hawkins, Beech, and Valtierra-Gallardo (Ref. 6) performed a series of experimental welds with a shielding gas of pure argon and different additions of nitrogen gas. The mixtures ranged from argon + 0.5% nitrogen to argon + 75% nitrogen. The results obtained are illustrated in Fig. 5. The results indicate the nitrogen content of the weld metal can be increased if the fraction of nitrogen in the shielding gas is increased.

The weld interface can then be visualized as a diffusion couple. Constant temperature is assumed for the sake of simplicity. The concentration of nitrogen into the base metal away from the weld interface can then be illustrated by the graph in Fig. 6.

The concentration of nitrogen is given by the following equation:

$$C = C_0 \text{erfc}\ \{x/[2(Dt)^{1/2}]\} \qquad (2)$$

where x is the distance from the weld interface, D is the diffusion coefficient for nitrogen in steel at a specific temperature and t is the time in seconds. C is the concentration of nitrogen at a distance x after time t, and C_0 is the concentration of nitrogen in the base plate. The distance between the weld interface and the intercept of the tangent to the graph in Fig. 6 is defined as the fusion distance and is given by $x = 2(Dt)^{1/2}$. These distances were calculated and are given in Table 2.

Diffusion distances for carbon can be calculated similarly (only the coefficient D is different). The calculated distances for carbon are shown in Table 3. The carbon content of the weld metal can be increased by simply welding with a filler metal with a higher carbon content. The results are shown graphically in Figs. 7 and 8.

Isothermal conditions are implicitly assumed in the above calculations. This assumption is in reality not valid, as the welded plate is cooling continuously. However, if the temperature sequence prediction from the Rosenthal equation (Ref. 4) in Fig. 9 is considered, the weld interface will be at a temperature higher than 1400°C for more than three seconds. Therefore, it was considered possible that a higher carbon or nitrogen content in the weld metal may increase the interstitial content of the HTHAZ significantly.

Table 2 — Diffusion Distances for Nitrogen in BCC-Iron at Different Temperatures

t (seconds)	1	2	3	4	6	8
x (a)	91	129	158	183	224	259
x (b)	100	142	174	202	247	285
x (c)	106	150	184	213	261	300

a = BCC-iron at 1300°C, b = BCC-iron at 1350°C, c = BCC-iron at 1380°C; x is in mm.

Table 3 — Diffusion Distances for Carbon in BCC-Iron at Different Temperatures

t (seconds)	1	2	3	4	6	8
x (a)	169	238	293	338	414	478
x (b)	189	267	328	378	463	535
x (c)	202	286	350	404	495	571

a = BCC-iron at 1300°C, b = BCC-iron at 1350°C, c = BCC-iron at 1380°C; x is in mm.

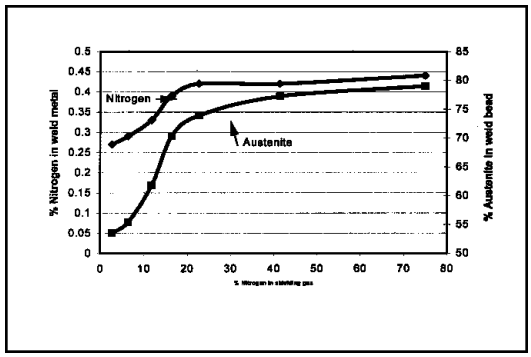

Fig. 5 — The nitrogen content and the percentage austenite in the weld metal as a function of the nitrogen content of the shielding gas during gas tungsten arc welding (Ref. 6).

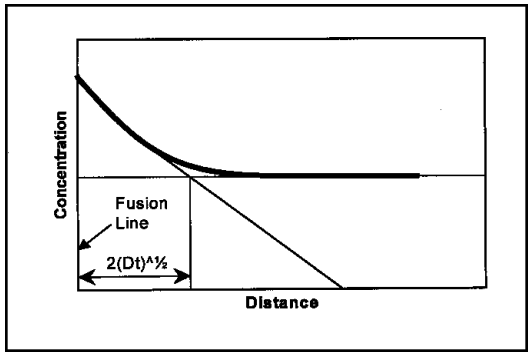

Fig. 6 — The concentration of nitrogen after diffusion for time t at a constant temperature (Ref. 7).

Experimental Welding and Results

Shielded Metal Arc Welding with E309L and E307 Electrodes

Shielded metal arc welding was done on 8-mm 3CR12 plate using an E309L electrode (0.03%C) and an E307 electrode (0.16%C), respectively. Welding was done parallel to the rolling direction. The ASTM grain size number of the remaining ferrite in the high-temperature heat-affected zone of the E307 welds was 4–5, while the grain size number of the remaining ferrite in the same region of the E309 welds was 1–2. A smaller ferrite grain size in the heat-affected zone of the E307 welds was thus observed. The grain size was determined by the use of the Hillards equation (a standard line intercept method). The microstructures of both high-temperature heat-affected zones consisted of ferrite and grain boundary martensite, with a higher fraction of grain boundary martensite in the E307 welds.

Both weld metal microstructures consisted of austenite and ferrite. The ferrite numbers (obtained from Fischer Fer-

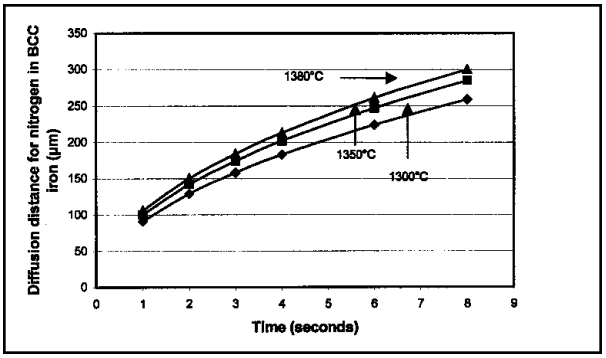

Fig. 7 — Calculated diffusion distances for nitrogen in BCC iron.

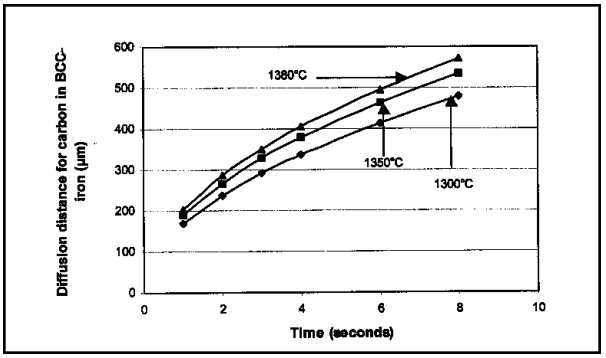

Fig. 8 — Calculated diffusion distances for carbon in BCC iron.

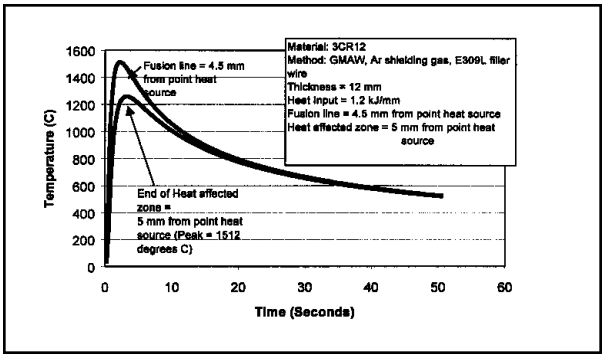

Fig. 9 — Temperature sequence prediction from the Rosenthal equation (Ref. 4).

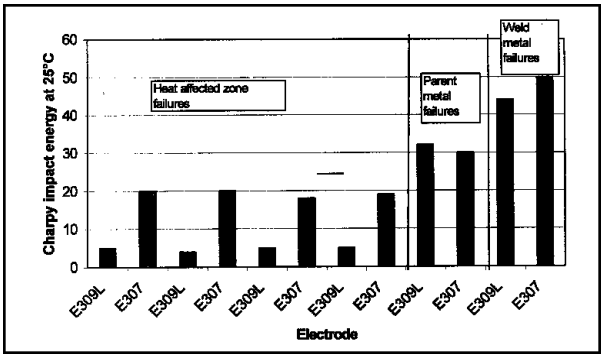

Fig. 10 — Charpy impact energy values at 25°C (SMAW, heat input = 0.7 kJ/mm).

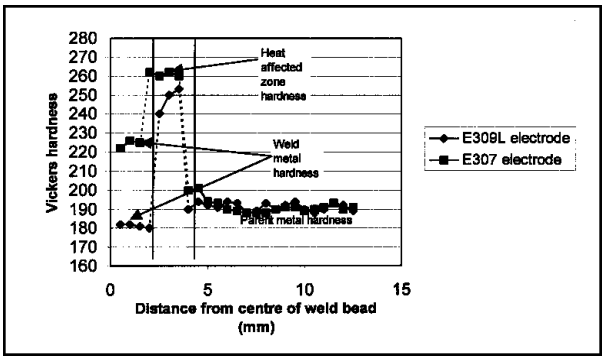

Fig. 11 — Hardness profile for welds in 8-mm 3CR12 (SMAW, heat input = 0.7 kJ/mm).

ritscope™ readings) were 15.5 FN in the weld metal of the E309L electrode and 13.1 FN in the same region of the E307 weld metal. Usually, a ferrite number of at least five is required in austenitic weld metals to prevent hot cracking during cooling.

All metallographic samples were prepared by polishing to a finish of 1 μm. Etching was done by quick swabbing with Kalling's No. 2 etching reagent.

The heat-affected zone hardness of the E307 weld is higher than the hardness in the same region of the E309L welds. This corresponds to the observed smaller grain size and larger fraction of grain boundary martensite. The absorbed Charpy impact energy is also higher for the heat-affected zone in the E307 welds than for the E309L welds, as can be seen in Fig. 10. The higher hardness, together with improved impact energy, may render the protection of the heat-affected zone by plastic deformation of the softer base metal and weld metal to be more likely (Ref. 2). This mechanism should increase the overall integrity of the weld in impact situations.

Half-size Charpy impact specimens (5 x 10 x 55 mm) were machined from each of the E309L and E307 welds. The specimens were cut across the weld beam, with the notch tip perpendicular to the rolling direction and the plate thickness on the 5-mm side. The notch tip was carefully directed into the high-temperature heat-affected zone with the notch tip parallel to the welding direction. Weld metal failures (crack located in the weld metal), base metal failures (crack located in the base metal), and heat-affected zone failures (crack located in the heat-affected zone) were observed, due to the fact that accurate placing of the crack tip in the heat-affected zone is not always possible. In the heat-affected zone failures of the E307 welds, the crack appeared to swerve away from the harder heat-affected zone into the base metal, resulting in higher absorbed Charpy impact energy values. Hardness profiles across the two different welds are shown in Fig. 11. The higher hardness of the 307 weld metal was expected due to the higher carbon content of the E307 electrode (0.16%) compared to that of the E309L electrode (<0.03%).

Gas Metal Arc Welding

Experimental gas metal arc welding (GMAW) was done on 12-mm hot-rolled 3CR12 plate. The heat input was held constant at 1.3 kJ/mm. Three separate welds were made using the following:

1) ER309L filler metal containing 0.03% carbon (1.2 mm) and pure argon shielding gas. The microstructure of the heat-affected zone is shown in Fig. 12.

2) ER307 filler metal containing 0.16% carbon and a pure argon shielding gas. The microstructure of the heat-affected zone is shown in Fig. 13.

3) ER309L filler metal containing

0.03% carbon (1.2 mm) and an argon +33% nitrogen shielding gas mixture. The microstructure of the heat-affected zone is shown in Fig. 14.

The weld metal microstructure of each of the welds consisted of austenite and ferrite. The average Fischer Ferritscope readings were 15.1 FN for the ER309L welds with pure argon shielding gas, 12.8 FN for the ER307 welds with pure argon shielding gas and 5.9 FN for the ER309L welds with the Ar-N_2 mixture. The low ferrite number of the weld with the Ar-N_2 mixture suggests that the nitrogen level in the ER309L weld metal was raised and that the austenite was stabilized by the higher nitrogen content. Although the ferrite number is still more than five, the susceptibility of the weld metal to hot cracking may be increased by the lower ferrite content.

The grain sizes in the heat-affected zones of the different welds were determined in a similar fashion as described earlier with the shielded metal arc welds. The average ASTM grain size number in the heat-affected zone of the ER309L weld with pure argon shielding gas was 1–2, while in the heat-affected zones of the ER309L welds with the Ar-N_2 shielding gas mixture and the ER307 welds with pure argon shielding gas, the average ASTM grain size number was 4–5. Therefore, a smaller ferrite grain size was observed in the heat-affected zones of the ER309L welds with the Ar-N_2 shielding gas mixture and the ER307 welds with pure argon shielding gas than in the heat-affected zone of the ER309L weld with pure argon shielding gas. In the heat-affected zones of the ER309L weld with the Ar-N_2 mixture and the ER307 weld, a larger fraction of grain boundary martensite was also observed. In accordance with these observations, the heat-affected zones of these two welds were harder than the heat-affected zone of the ER309L weld with pure argon shielding gas. Hardness profiles across these welds are shown in Fig. 15. Contrary to expectation, the ER307 weld metal hardness is only marginally higher than that of the ER309L. This may be due to the fact higher peak temperatures are reached in GMAW as compared with SMAW, and, consequently, the interstitial elements could diffuse out of the weld metal faster than during SMAW.

The smaller grain size in the heat-affected zones of the ER309L weld with the Ar-N_2 mixture and the ER307 weld with the pure Ar shielding gas, together with the higher hardness, would render the protection of the zone by the softer weld metal and base metal to be more likely in impact situations (Ref. 2), and would increase the overall integrity of the weld. Similar to the SMAW specimens discussed previously, three types of failures were observed in the full-size Charpy specimens (10 x 10 x 55 mm) machined from the welds. The notch was placed perpendicular to the rolling direction and the plate thickness. Proper Charpy specimens could not be obtained from the Ar-N_2 welds because of the excessive spatter that occurred in these welds. The spatter is similar to that observed when shielding gas flow is insufficient to prevent air contamination of the shielding gas, and may therefore be directly attributed to the nitrogen present in the shielding gas. As a result, only the ER309L and ER307 welds (both with pure argon shielding gas) were evaluated. The results are shown in Fig. 16. Higher impact energies are observed in Fig. 16 than in Fig. 10, due to the fact full-size Charpy specimens were used instead of the half-size specimens used with the shielded metal arc welds.

Chemical Analysis

Chemical analysis of the base metal, weld metal, and heat-affected zone was done to confirm the transfer of carbon and nitrogen across the weld interface. The heat-affected zone samples were obtained from very fine drillings (0.5-mm-diameter drill) from lightly etched specimens. Etching was done by quick swabbing with Kalling's nr. 2. The results are tabulated in Table 4.

The high levels of carbon (HTHAZ of ER307 + Ar) and nitrogen (ER309L + Ar-N_2) suggest that interstitial diffusion of carbon and nitrogen may have taken place. Contamination of the heat-affected zone samples from either the weld metal or the base metal was inescapable but care was taken to take the drilling as far as possible from the weld metal to get contamination from a region with a lower interstitial content rather than from the weld metal with the higher carbon and nitrogen content. The results nevertheless show an increase of 96% in carbon content and 78% in nitrogen content. The large increase in interstitial content suggests that contamination of the sample drillings of the heat-affected zone by the weld metal may have influenced the result of the chemical analysis.

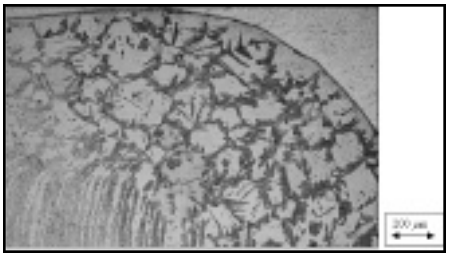

Fig. 12 — The microstructure of the heat-affected zone in 3CR12 (GMAW, 1.3 kJ/mm, ER309L filler metal, argon shielding, 100X).

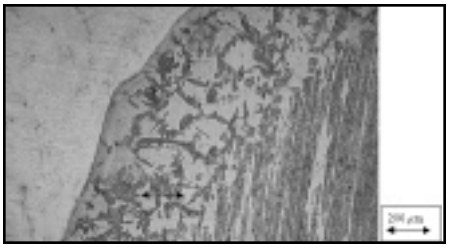

Fig. 13 — The microstructure of the heat-affected zone in 3CR12 (GMAW, 1.3 kJ/mm, ER307 filler metal, argon shielding, 100X).

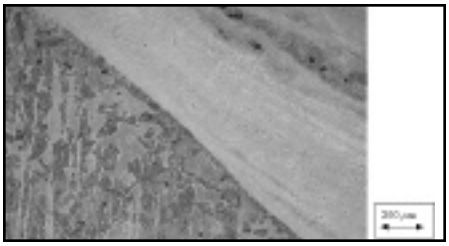

Fig. 14 — The microstructure of the heat-affected zone in 3CR12 (GMAW, 1.3 kJ/mm, ER309L filler metal, argon-nitrogen shielding, 100X).

Continuous Cooling and Diffusion

It was mentioned earlier that the isothermal conditions assumed in the diffusion distance calculations were not valid, since the welded plate cools continuously. In order to get a more acceptable model of the interstitial diffusion of car-

Table 4 — Carbon and Nitrogen Contents in Different Zones of Welds in 3CR12

Process (welding wire and shielding gas)	Base Metal %C	Base Metal %N	Heat-Affected Zone %C	Heat-Affected Zone %N	Weld Metal %C	Weld Metal %N
ER309L + Ar	0.029	0.019	0.031	0.018	0.032	0.024
ER309L + Ar-N_2	0.033	0.018	0.028	**0.050**	0.032	0.092
ER307 + Ar	0.027	0.017	**0.053**	0.019	0.130	0.020

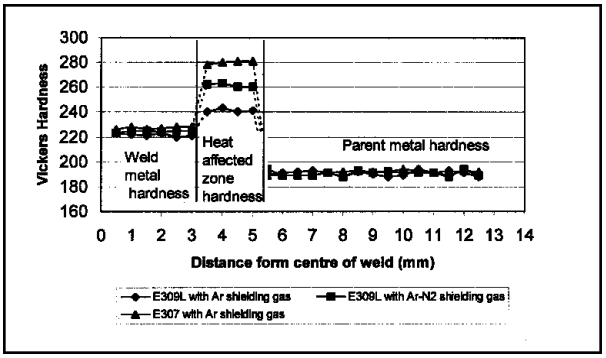

Fig. 15 — Hardness profile for welds in 12-mm 3CR12 (GMAW, heat input = 1.3 kJ/mm).

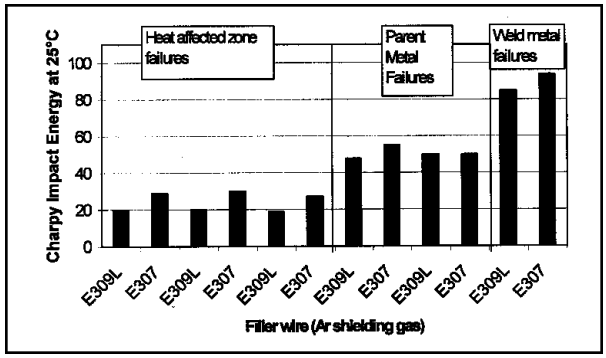

Fig. 16 — Charpy impact values at 25°C (GMAW, heat input = 1.3 kJ/mm).

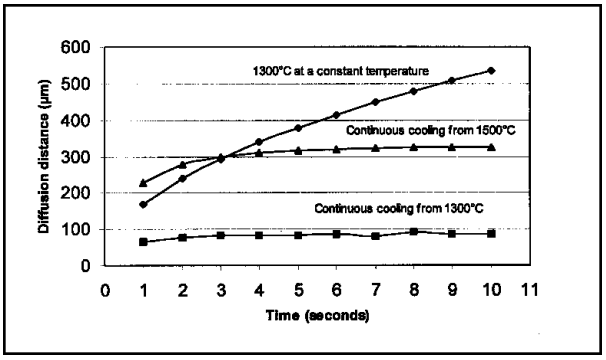

Fig. 17 — Diffusion distance calculated for carbon in 3CR12 for a constant temperature of 1300°C and continuous cooling from 1300°C and 1500°C.

bon during the cooling period of a weld, a temperature sequence for the weld interface (1500°C) of a 1.0 kJ/mm weld in 12-mm 3CR12 plate was constructed from the Rosenthal equation (Ref. 4). In order to construct the sequence, a period of 40 s was divided into time intervals of 0.1 s. The diffusion coefficient was calculated at the end of each interval, using the temperature at that time. The average diffusion coefficient was then determined after 1-s intervals up to 10 s.

The results of these calculations are shown in Fig. 17, together with the earlier results when isothermal conditions were assumed. The continuous cooling has a definite decreasing effect on the theoretical diffusion distance. The results as discussed earlier predict a diffusion distance of 479 µm after 8 s and 535 µm after 10 s, at a constant temperature of 1300°C. On the other hand, continuous cooling from 1300°C only predicts a diffusion distance of 85 µm after 10 s.

If the weld interface is assumed to form at 1500°C (the approximate melting point of 3CR12), and continuous cooling as predicted by the Rosenthal equation (Ref. 4) is taken into account, the theoretical diffusion distance is 326 µm after 10 s. The microstructural changes and the difference in impact properties as observed in the experimental welds discussed earlier therefore seems to be the result of interstitial diffusion from the weld metal into the base plate across the weld interface.

Conclusions

Ferrite grain growth in the heat-affected zones of welds in 3CR12 has a detrimental effect on the impact properties of the welded joint. Ferrite grain growth can be inhibited by increasing the amount of grain boundary austenite in the heat-affected zone at high temperatures. Increasing carbon or nitrogen contents in the heat-affected zone should act to stabilize grain boundary austenite. Consequently, a decrease in ferrite grain growth should be observed in the heat-affected zone of 3CR12 welds.

A decrease in the ferrite grain size occurs in the heat-affected zones of welds in 3CR12 if the carbon or nitrogen content of the weld metal is increased. The finer heat-affected zone structure improves the impact properties of the welded joint. Diffusion distance calculations suggest that the finer structure, increase in grain boundary austenite, and improvement in impact properties are the result of diffusion of carbon and nitrogen from the weld metal, across the weld interface and into the heat-affected zone. Although an increase in the interstitial content of the heat-affected zone was observed in chemical analysis, contamination of the heat-affected zone samples by the weld metal could not be ruled out. Therefore, the chemical analysis should not be viewed as conclusive. A filler metal with a different interstitial content, however, may conclusively alter the phase composition of the heat-affected zone.

References

1. Product Guide for 3CR12. 1988. Middelburg Steel and Alloys (Pty) Limited, (1): 14–19.

2. Grobler, C. 1987. Weldability studies on 12% and 14% chromium steels. Ph.D., pp. 62–79 and 86–122.

3. Zaayman, J. J. J. 1992. The heat-affected zone toughness of welds in 11 to 12 per cent chromium steels. M. Eng. (UP), pp. 31–71 and 76–93.

4. Easterling, K. 1993. Introduction to the Physical Metallurgy of Welding. Butterworth, Heinemann; Oxford, Second Edition 1992, Second Impression 1993, pp. 1–38.

5. Gooch, T. G., and Ginn, B. J. 1988. Heat-affected zone toughness of MMA welded 12%Cr martensitic-ferritic steels. Report from the cooperative research program for research members only. The Welding Institute, Cambridge, England, pp. 3–30.6.

6. Hawkins, D. N., Beech, J., and Valtierra-Gallardo, S. 1988. A new approach to microstructural control in duplex stainless steel welds, Sheffield, pp. 199–203.

7. Guy. A. G. 1972. Introduction to Materials Science. NewYork, N.Y.: McGraw-Hill Book Co.